# Diffusive Shock Re-Acceleration

**Damiano Caprioli[1,2]†, H. Zhang[2] and A. Spitkovsky[2]**

[1]Department of Astronomy and Astrophysics, University of Chicago,
5640 S Ellis Ave, Chicago, IL 60637, United States

[2]Department of Astrophysical Sciences,
Princeton University, 4 Ivy Ln., Princeton, NJ 08544, United States

(Received xx; revised xx; accepted xx)

CONTENTS



† Email address for correspondence: caprioli@uchicago.edu

**Disclaimer:** This manuscript is just a draft of a work in progress. It contains typos and unrevised sections, but main ideas and plots are outlined for the discussion's sake.

**Abstract:** We have performed 2D hybrid simulations of non-relativistic collisionless shocks including pre-existing energetic particles ("seeds") to study the reacceleration of Galactic cosmic rays (GCRs) in supernova remnant (SNR) shocks and of solar wind energetic particles in heliospheric shocks. Energetic particles can be effectively reflected and accelerated regardless of the shock inclination via a process that we call diffusive shock re-acceleration (DSRA). We find that reaccelerated seeds can excite the Bell instability and drive efficient magnetic field amplification, eventually triggering the injection of thermal protons even in shock configurations where it is normally suppressed. We also characterize the current in reflected seeds, finding that it tends to a universal value $J \simeq n_{\rm CR} v_{\rm CR}$, where $n_{\rm CR}$ and $v_{\rm CR}$ are the seed density and velocity. Finally, we apply our findings to SNR shocks propagating in the typical interstellar medium, finding that the reacceleration of GCRs may drive the Bell instability in less than $\sim 10$yr and contribute to the overall particle acceleration for middle-age SNRs.

## 1. Introduction

Collisionless shocks are ubiquitous in space and astrophysical environments, and are always associated with non-thermal particle and emission. Important examples are non-relativistic shocks at SNR blast waves, which are widely regarded as the sources of Galactic CRs (Morlino & Caprioli 2012; Caprioli *et al.* 2010), and heliospheric shocks, privileged laboratories where to study particle acceleration thanks to in-situ spacecraft observations.

In the past few years, modern supercomputers have opened a new window for investigating the non-linear interaction between accelerated particles and electromagnetic fluctuations from first principles via kinetic particle-in-cell simulations. A crucial contribution to the present understanding of particle acceleration at non-relativistic shocks came from hybrid (kinetic ions–fluid electrons) simulations, which allow to fully capture the ion dynamics and the development of plasma instabilities at a fraction of the computational cost required to follow also the electron dynamics. For an outline of the most important results obtained with such hybrid simulations, see the recent review by Caprioli (2015).

In this paper we want to generalize such results to the cases in which the shock runs into a medium that is already filled with energetic seed particles, as it is typically the case of the interstellar medium or the solar wind. This is a crucial step towards a better understanding of interstellar and heliospheric shocks, whose observed phenomenology is not always explained in terms of the most common acceleration mechanism, namely diffusive shock acceleration (DSA). After a brief introduction about how diffusive shock acceleration (DSA) occurs for shocks propagating at a different angles with respect to the large-scale magnetic field, in §2 we discuss the injection and acceleration of pre-existing energetic seeds for oblique shocks; in particular, we address the triggering of the Bell instability driven by the current in reflected CRs, which has a crucial back-reaction on the global shock structure. In §3 we study the (re)acceleration efficiency of both seeds and thermal protons for different shock inclinations, comparing the results with and without energetic seeds. The very general properties of the current in reflected CRs are worked out and discussed in §4. Finally, in §5 we put our findings in the context of re-acceleration of Galactic CRs seeds in SNR shocks before concluding in §6.

## 2. Hybrid Simulations with Energetic Seeds

### 2.1. *DSA and Shock Inclination*

A crucial parameter that controls how efficiently a shock can channel kinetic energy into non-thermal particles is its inclination, defined by the angle $\vartheta$ between the direction of the large-scale magnetic field $\mathbf{B}_0$ and the shock normal, such that $\vartheta = 0^\circ$ ($\vartheta = 90^\circ$) corresponds to parallel (perpendicular) shocks; in the following we also use *oblique* for shocks with $45^\circ \lesssim \vartheta \lesssim 70^\circ$.

In Caprioli & Spitkovsky (2014*a*) we found the acceleration of thermal ions is efficient at quasi-parallel shocks: more than 10% of the shock ram kinetic energy can be converted in energetic particles with the universal power-law tail predicted by the DSA theory. For oblique shocks, such an acceleration efficiency is suppressed and becomes negligible above $\vartheta = 60^\circ$. The motivation is discussed in Caprioli *et al.* (2015), where we outlined how ion injection is controlled by reflection off the shock electrostatic barrier, which oscillates on a cyclotron timescale, and the shock inclination. Protons are injected into DSA if, after they are specularly reflected at the shock barrier, have a minimum energy $E_{\rm inj}(\vartheta)$ that is an increasing function of $\vartheta$. In order to achieve such an injection energy, protons must be reflected by the shock (and gain energy via shock drift acceleration, SDA) a certain number $N$ of times, but at each encounter with the reforming shock barrier they have a probability of $\sim 75\%$ to be advected away downstream; therefore, the fraction of particles that can undergo $N$ SDA cycles is only $\sim 0.25^N$. We also found that for $\vartheta \lesssim 45^\circ$ the injection energy is $\sim 10 E_{\rm sh}$, which is achieved with $N \simeq 3$ SDA cycles, returning an injection fraction of $\sim 1\%$, in good agreement with simulations (Caprioli *et al.* 2015). For larger shock inclinations, however, $N \gtrsim 3$ and the fraction of injected ions drops exponentially with $\vartheta$. When the injection fraction is about 1%, the current in energetic particles is large enough to drive a very effective amplification of the initial magnetic field configuration (Caprioli & Spitkovsky 2014*b*), which cannot happen for $\vartheta \gtrsim 50^\circ$, instead. The net result is that quasi-parallel shocks can *spontaneously* inject particles from thermal energies thereby leading to a very efficient DSA and magnetic field amplification, while more oblique shocks do not exhibit any non-thermal activity.

### 2.2. *Hybrid Simulation Setup*

In this section we investigate how the presence of seeds with an initial energy exceeding $E_{\rm inj}$ may overcome the injection problem for oblique shocks. We use the massively-parallel code *dHybrid* to run simulations of non-relativistic shocks including pre-energized particles. Simulations are 2D, but we account for the three spatial components of the particle momentum and of the electric and magnetic fields. As usual, we normalize lengths to the proton skin depths $c/\omega_p$, where $c$ is the speed of light and $\omega_p \equiv \sqrt{4\pi n_p e^2/m}$ is the proton plasma frequency, with $m, e$ and $n_p$ the proton mass, charge and number density; time is measured in units of inverse proton cyclotron frequency $\omega_c^{-1} \equiv mc/eB_0$, where $B_0$ is the strength of the initial magnetic field; finally, velocities are normalized to the Alfvén speed $v_A \equiv B/\sqrt{4\pi mn}$, and energies to $E_{sh} \equiv m v_{\rm sh}^2/2$, with $v_{\rm sh}$ the velocity of the upstream fluid in the downstream frame, which is also the simulation frame. Shocks are produced by sending a supersonic flow against a reflecting wall and are characterized by their sonic and Alfvénic Mach numbers $M_s \equiv v_{\rm sh}/c_s$, $M_A \equiv v_{\rm sh}/v_A$, with $c_s$ the sound speed. Fluid electrons have a polytropic equation of state with an effective adiabatic index chosen in order to satisfy the Rankine–Hugoniot conditions imposing thermal equilibration between downstream ions and electrons (see Caprioli & Spitkovsky 2013, 2014*a*, for more details).

The novel ingredients in the simulations presented here is the presence of an additional

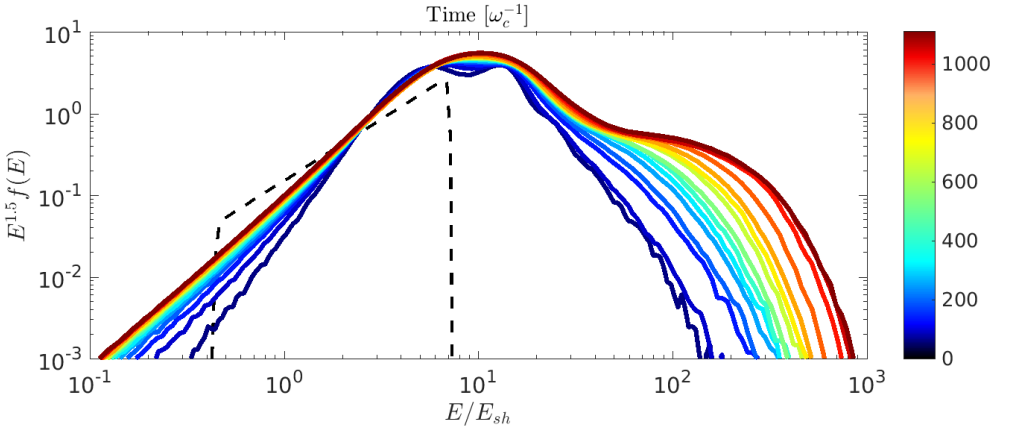


FIGURE 1. Time evolution of the downstream CR energy spectra (see colorbar) for our benchmark shock with $\vartheta = 60°$, $M = 30$, and seeds with $v_{\rm CR} = 50 v_A$ and $n_{\rm CR} = 0.01$. The dashed black line shows the initial energy spectrum of CR seeds. Spectra are multiplied by $E^{1.5}$ to demonstrate agreement with DSA theory. The growth of the maximum energy and the flattening of the power law tail shows that energetic CRs are injected into DSA, even in an oblique shock where thermal ions cannot be injected.

population of energetic seeds, initialized in the upstream reference frame as isotropic and with a flat distribution in each momentum component $p_i$ on the range $-mv_{\rm CR} \leqslant p_i \leqslant mv_{\rm CR}$, which corresponds to an average energy of $(v_{\rm CR}/v_{\rm sh})^2 E_{\rm sh}$; in the simulation frame such an isotropic population is also drifting along with the thermal ions with velocity $v_{\rm sh}$. We refer to this component either as "seeds" or "CRs" throughout the paper. For the CRs the left side of the box is open (and not a reflective wall) to prevent the formation of an additional shock on the CR scales.

As a benchmark run, we consider a strong shock with $M_s \simeq M_A \equiv M = 30$ and $\vartheta = 60°$, a configuration where thermal ions are hardly injected (Caprioli & Spitkovsky 2014*a*). The time-step is chosen as $\Delta t = 0.0015\omega_c^{-1}$ and the computational box measures $[L_x, L_y] = [10^5, 500] c/\omega_p$, with two cells per ion skin depth and four particles per cell for both protons and CRs. The CRs drift with the incoming flow into the shock and have $v_{\rm CR} = 50 v_A$ and $n_{\rm CR} = 0.01$, so that the energy density in CRs is negligible ($\lesssim 3\%$) with respect to that in thermal protons. We will discuss later in the paper how results depend on the choice of $M$, $\vartheta$, $v_{\rm CR}$, and $n_{\rm CR}$ .

### 2.3. *Cosmic Ray Injection and Re-Acceleration*

Fig. 1 shows that the post-shock CR spectrum (integrated over the whole downstream), initially peaked around $10 E_{\rm sh}$, develops a DSA power-law tail whose extent (the exponential cutoff at high energies) increases with time. For strong shocks, the universal DSA momentum spectrum is $f(p) \propto p^{-4}$, which translates into an energy spectrum $f(E) = 4\pi p^2 f(p) \frac{dp}{dE}$. Since for non relativistic CRs (as in our case) $p \propto E^{1/2}$, we expect $f(E) \sim E^{-1.5}$, and the CR energy distribution $f(E)$ in Fig. 1 converges to the theoretical slope. The fraction of CRs in the non-thermal tail is $\gtrsim 10\%$, much larger than the typical fraction of $\lesssim 1\%$ of protons that get injected and accelerated via DSA. Finally, at late times the low-energy part of the spectrum relaxes towards a Maxwellian-like distribution because of collisionless interactions mediated by the self-generated magnetic turbulence.

We stress that for such an oblique shock we do not either expect an effective injection of *thermal* protons into DSA, because the fraction of them that can achieve the injection

energy $E_{\rm inj}$ via SDA is very small. More precisely, particle injection into DSA requires a minimum velocity along and transverse to the shock normal to allow particles to overrun the shock and escape upstream (see Caprioli *et al.* 2015, fig. 4). CR seeds differ from thermal ions for three reasons:

- The shock barrier is regulated by thermal protons and cannot prevent energetic CRs from propagating between the two sides of the shock, similarly to what happens for ions with large mass/charge ratio (Caprioli *et al.* 2017);
- Without interaction with the shock surface, SDA does not occur and CRs can be directly injected into DSA if their velocity exceeds the one required for overrunning the shock (Caprioli *et al.* 2015);
- CRs are significantly "hotter" than protons, in the sense that their phase space distribution is much more isotropic than that of the supersonic thermal particles; therefore, CRs can impinge on the shock with larger velocities transverse to the shock normal, which enhances their chances to overrun the shock compared to cold incoming beams.

In our benchmark case, the composition of $\mathbf{v}_{\rm CR}$ and $\mathbf{v}_{\rm sh}$ gives rise to CRs impinging on the shock with energies as large as $\sim (v_{\rm CR}+v_{\rm sh})^2/v_{\rm sh}^2 E_{\rm sh} \sim 7E_{\rm sh}$ (dashed line in Fig. 1). After reflection at the shock, such an energy increases by another factor of $\sim 2$ thanks to the typical energy gain for Fermi acceleration $\Delta E/E \approx \frac{4}{3}v_{\rm sh}/v$, as illustrated by the second peak at $E \gtrsim 10E_{\rm sh}$ visible at early times in Fig. 1. Quite intriguingly, at late times the non-power-law part of the CR distribution resembles a Maxwellian, with an effective "temperature" of $T_{\rm CR,eff} \simeq 15E_{\rm sh}$, corresponding to the characteristic energy of CRs that underwent one cycle of Fermi acceleration at their first shock encounter.

Particles with such a large energy can overrun the shock be injected into DSA even for oblique shocks. We name this process *Diffusive Shock Re-Acceleration* (DSRA) because it differs from DSA in two respects: 1) The fraction of injected particles is not a function of the shock inclination only, as it is the case for thermal particles (Caprioli *et al.* 2015), but also depends on the velocity of the seeds; 2) The spectrum produced by such an acceleration is not the universal $p^{-4}$ expected for DSA at strong shocks, but rather the flatter between the DSA spectrum and the initial seed spectrum (Bell 1978; Blasi 2004).

### 2.4. *DSRA Back-reaction*

DSA is always associated with an anisotropic population of energetic particles in the upstream, which drives a rearrangement or even an amplification of the background magnetic field (Caprioli & Spitkovsky 2014*b*; Amato & Blasi 2009). The main instabilities responsible for such amplification are the resonant streaming instability (e.g., Skilling 1975; Bell 1978) and the non-resonant hybrid (or Bell) instability (Bell 2004). The former is typical of moderately-strong shocks with $M \lesssim 30$ and saturates at quasi-linear levels od field amplification $\delta B/B_0 \lesssim 1$, while for stronger shocks the Bell instability can generate very non-linear fluctuations $\delta B/B_0 \gg 1$ (Caprioli & Spitkovsky 2014*b*).

We now consider the effects of the current carried the CRs reaccelerated by the shock. Such a current drives the Bell instability, which amplifies the initial $\mathbf{B}_0$ field and distorts its initially-oblique configuration, creating "pockets" of quasi-parallel field regions upstream of the shock, which locally allow the injection of thermal protons. Fig. 2 shows the local magnetic field inclination around the shock for $t = 153\omega_c^{-1}$ and $t = 453\omega_c^{-1}$ for our benchmark run. The initial field inclination ($\vartheta = 60°$) is drastically rearranged, with quasi-parallel regions (in blue) appearing upstream of the shock in filamentary structures. Such filamentary structures, which start as small-wavelength perturbations, grow with time in such a way that their transverse scale is comparable with the gyroradius of the highest-energy diffusing particles, which carry most of the

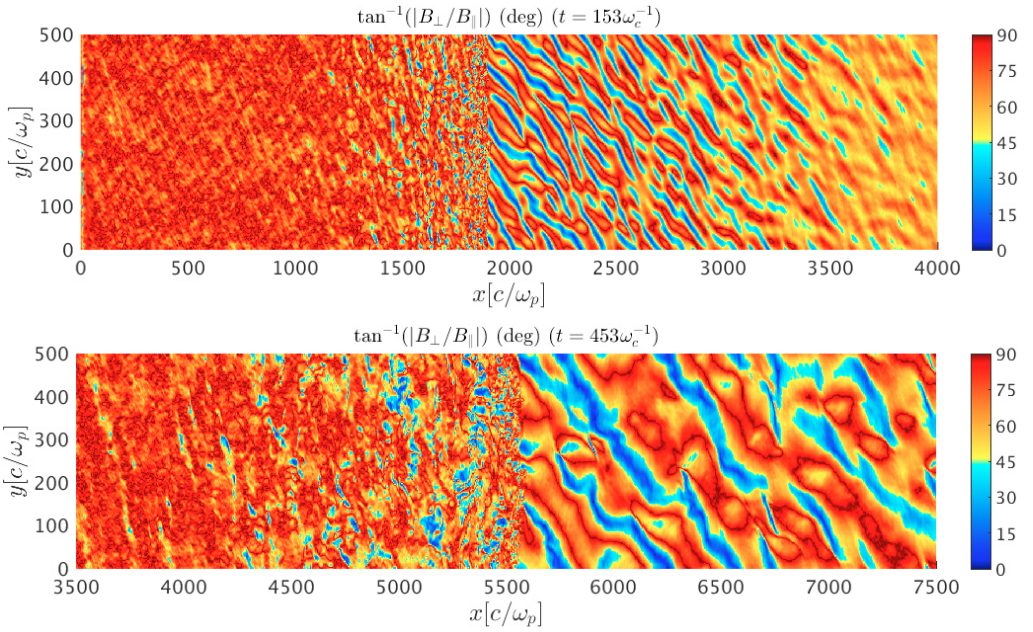


FIGURE 2. Local magnetic field inclination around the benchmark shock with $\vartheta = 60°$, $M = 30$, $v_{\rm CR} = 50v_A$, and $n_{\rm CR} = 0.01$ at $t \simeq 150\omega_c^{-1}$ and $t \simeq 50\omega_c^{-1}$ (top and bottom panels). The Bell instability driven by re-accelerated CRs distorts the initial oblique field and creates quasi-parallel pockets (blue regions) where protons can be injected into DSA. The transverse size of such quasi-parallel filaments grows with time (e.g., Reville & Bell 2013; Caprioli & Spitkovsky 2013).

current (Caprioli & Spitkovsky 2013, 2014*b*; Reville & Bell 2013). The two panels in Fig. 2 attest to this increase in wavelength with time.

The presence of patches of quasi-parallel magnetic field created in the non-linear stage of the Bell instability creates the conditions for the injection and acceleration also of thermal protons. Fig. 3 shows the evolution of the downstream proton spectra for our benchmark run. The expected Maxwellian distribution (black dashed line) fits the low-energy thermal part of the spectrum well at all the times. Supra-thermal protons with $2E_{\rm sh} \lesssim E \lesssim 10E_{\rm sh}$ are generated at the shock via shock-drift acceleration (SDA), as discussed in Caprioli *et al.* (2015), and at early times form a "bump", which remains stationary in the absence of CR seeds (Caprioli & Spitkovsky 2014*a*). In our case, instead, the fraction of supra-thermal ions with decreases with time, while non-thermal power-law tail develops and grows with time. This suggests that supra thermal ions can be injected into the DSA process where the shock inclination is reduced below $\vartheta \sim 50°$ (Caprioli *et al.* 2015). The fraction of injected protons ($\sim 10^{-3}$) is significantly smaller than for quasi-parallel shocks, but the fraction of the post shock energy density in protons with $E \gtrsim 10E_{\rm sh}$ (hereafter, the acceleration efficiency $\varepsilon_{\rm p}$) reaches a value of $\varepsilon_{\rm p} \sim 3\%$, to be compared to less than 0.5% for a shock with $M = 30$ and $\vartheta = 60°$ without CR seeds (Caprioli & Spitkovsky 2014*a*).

### 2.5. *The Onset of the Bell instability*

To better outline the effect of the CR-induced streaming instability on proton acceleration, we vary the initial CR density and check how the onset of the Bell instability and the trigger of proton injection depends on $n_{\rm CR}$. The typical growth time of the Bell

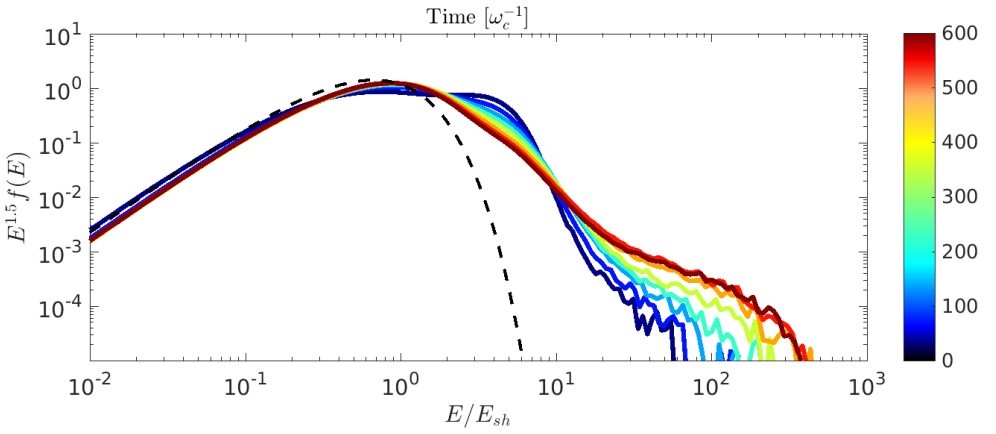


FIGURE 3. As in Fig. 1, but for the proton energy spectrum. Protons develop a non-thermal tail after the onset of the Bell instability ($t \gtrsim 100\omega_c^{-1}$), which opens up quasi-parallel patches at the shock surface (see Fig. 2) where thermal particles can be injected. The dashed line corresponds to the Maxwellian distribution estimated with standard Rankine–Hugoniot conditions. Note how the supra-thermal "bump" (protons with energies $2E_{\rm sh} \lesssim E \lesssim 10E_{\rm sh}$) decreases with time while the non-thermal tail grows, which indicates the injection of SDA protons into DSA.

instability (in the MHD limit) is given by

$$\tau_{\rm Bell} = 4\pi \frac{n_p v_A}{J^r_{\rm CR}} \omega_c^{-1} \tag{2.1}$$

where we introduced

$$J_{\rm CR} \equiv \chi e n_{\rm CR} v_{\rm sh}. \tag{2.2}$$

as the current in reflected CRs. $\chi$ parametrizes $J_{\rm CR}$ in units of $n_{\rm CR} v_{\rm sh}$ and represents a measure of the initial reflectivity of the shock; we expect it to depend on $v_{\rm CR}$ and on $\vartheta$, but not on $n_{\rm CR}$, and to change in time only once the magnetic field amplification has reached non-linear levels. By measuring the current in reflected CRs from simulation we find that $\chi \sim 1$ (details are provided in §4), so that for our benchmark run

$$\tau_{\rm Bell} \sim 80 \left(\frac{n_{\rm CR}}{0.01}\right)^{-1} \omega_c^{-1}. \tag{2.3}$$

We consider the case of a shock with the same benchmark parameters except that we pose $n_{\rm CR} = 2 \times 10^{-3}$ instead of $n_{\rm CR} = 0.01$; therefore, the Bell instability is expected to develop a factor of 5 later in time according to Eq. 2.3, also leading to a later trigger of proton injection into DSA. Fig. 4 shows the time evolution of the acceleration efficiency $\varepsilon_{\rm CR}$ and of the effective inclination of the magnetic field at the shock for $n_{\rm CR} = 0.01$ and $n_{\rm CR} = 2 \times 10^{-3}$. The proton acceleration efficiency $\varepsilon_{\rm CR} \lesssim 1.5\%$ until $\tau_{\rm Bell}$, when the Bell instability starts to produce patches of quasi-parallel ($\vartheta \lesssim 45°$) field. The correlation between the onset of the Bell instability (in agreement with the theoretical prediction) and the increase in the proton acceleration efficiency demonstrates the crucial role of CR seeds in triggering proton DSA.

We conclude that, in the presence of energetic seeds, there is a typical timescale determined by the current in reflected CRs ($\tau_{\rm Bell}$) after which the initial oblique magnetic field configuration is rearranged and thermal protons can be injected into DSA even at oblique shocks. In order to keep such a typical timescale within the range of accessibility of modern supercomputers, we use CR density much larger than those expected in the interstellar medium or in the solar wind, but we show in §5 that the extrapolation of

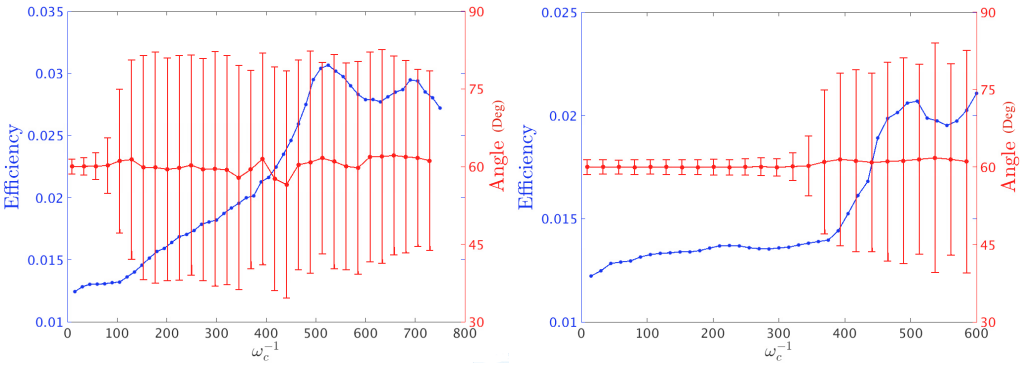


FIGURE 4. Time evolution of the proton acceleration efficiency $\varepsilon_{\rm CR}$ (left axes, blue) and of the effective shock inclination (right axes, red), for $n_{\rm CR} = 0.01$ and $n_{\rm CR} = 2 \times 10^{-3}$ (left and right panel, respectively). Error bars in the field inclination account for one standard deviation from the average, which is constant at the initial value of $\vartheta = 60°$. Note how $\varepsilon_{\rm CR} \lesssim 1.5\%$ until the onset of the Bell instability, which occurs later for the lower value of $n_{\rm CR}$.

$\tau_{\rm Bell}$ to astrophysical environments makes the effect relevant, for instance, for supernova remnant (SNR) shocks.

## 3. Acceleration Efficiency: Dependence on Shock Inclination

Thus far, our results show that energetic CRs are reaccelerated in oblique shocks with $\vartheta = 60°$, and that in this case the proton acceleration efficiency is boosted to a few per cent level. We investigate how CR re-acceleration and proton acceleration depend on the shock inclination by performing a series of 2D runs with $M = 30$ with different field inclinations from 0° to 80° (see Tab. 1). Since at more oblique shocks a larger injection energy is required, we chose larger values of $v_{\rm CR}$ to ensure that reflected CRs can be injected into DSRA, but keep the product of $v_{\rm CR}$ and $n_{\rm CR}$ roughly constant in order to have the same current $J_{\rm CR} \simeq e n_{\rm CR} v_{\rm CR}$ in all the runs. The timestep $dt$ is then fixed accordingly to satisfy the Courant condition for CRs. In all the runs the initial CR energy density fraction $\lesssim 5\%$ to ensure that the CRs are energetically underdominant with respect to protons.

### 3.1. *CR Reacceleration Efficiency*

In addition to the proton acceleration efficiency $\varepsilon_{\rm p}$, defined as the fraction of the post-shock energy density in ions with $E > 10 E_{\rm sh}$, one could introduce the CR acceleration efficiency $\varepsilon_{\rm CR}$ defined as the ratio of the total CR energy to the total energy in the downstream (which is dominated by the thermal protons). Such an absolute value, however, is not physically meaningful because it scales linearly with $n_{\rm CR} v_{\rm CR}^2$, which is typically much smaller than $n_p v_{\rm sh}^2$ in realistic astrophysical environments. For our benchmark case ($n_{\rm CR} = 0.01$, $v_{\rm CR} = 50 v_A$, $\vartheta = 60°$) we find that the post-shock energy ratio between CRs and thermal protons is about 12%, a factor of $\sim 4$ more than far upstream. Such a factor of 4 can be interpreted by considering that for $v_{\rm CR} \gtrsim v_{\rm CR}$ the downstream seed density increases by the shock compression ratio $\sim 4$, while their velocity is not reduced as the one of the bulk flow.

Fig 5 shows that the CR acceleration efficiency $\varepsilon_{\rm CR}$ does not depend greatly on the inclination angle for the runs with parameters in Tab. 1, being always between 10%

| Shock Inclination | $\Delta t$ ($\omega_c^{-1}$) | $[L_x, L_y]$ ($c/\omega_p$) | $v_{\rm CR}$ ($v_A$) | $n_{\rm CR}(n_p)$ |
|---|---|---|---|---|
| 0° | 0.0015 | [20,000, 200] | 50 | 0.01 |
| 30° | 0.0015 | [20,000, 200] | 50 | 0.01 |
| 45° | 0.0015 | [20,000, 200] | 50 | 0.01 |
| 50° | 0.0015 | [40,000, 200] | 50 | 0.01 |
| 60° | 0.0015 | [40,000, 300] | 50 | 0.01 |
| 70° | 0.001 | [30,000, 200] | 90 | 0.006 |
| 80° | 0.0005 | [30,000, 200] | 200 | 0.0013 |

TABLE 1. Parameters for the 2D simulations of §3. All the shocks have $M = 30$.

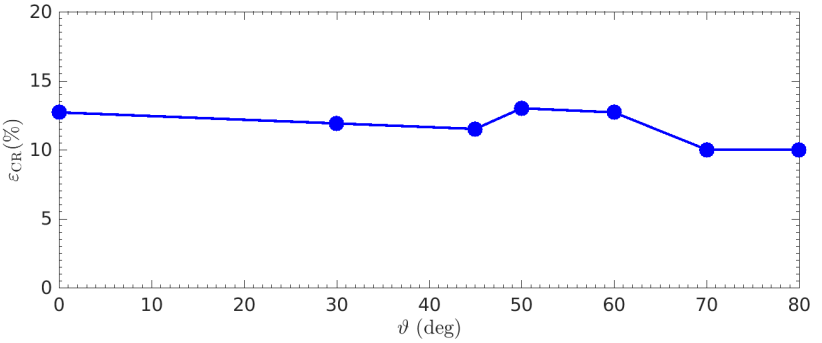


FIGURE 5. CR re-acceleration efficiency $\varepsilon_{\rm CR}$ as a function of the shock inclination at $M = 30$ (see Tab. 1 for the run parameters). The absolute value of $\varepsilon_{\rm CR}$ has no intrinsic physical meaning because it scales linearly with $n_{\rm CR}v_{\rm CR}^2$, but the fact that CR DSRA efficiency is independent of the shock inclination is a general result.

and 12%. The absolute values of $\varepsilon_{\rm CR}$ are rescaled to their values at $n_{\rm CR} = 0.01$ and $v_{\rm CR} = 50v_A$ to allow for comparison between runs with different $v_{\rm CR}$ and $n_{\rm CR}$.

### 3.2. *Ion Acceleration Efficiency*

Fig. 6 illustrates the ion acceleration efficiency $\varepsilon_{\rm p}$ for different shock inclinations in the presence of CR seeds (blue line). With respect to the case without CRs (fig. 3 of Caprioli & Spitkovsky 2014*a*), we individuate three regimes characterized by the effectiveness of the Bell instability in producing quasi-parallel regions in front of the shock. The red line in Fig. 6 shows the effective shock inclination after $\tau_{\rm Bell}$ in each run.

• Regime A, $\vartheta \leqslant 45°$: protons can be injected from the thermal bath and diffuse off magnetic turbulence created by self-generated streaming instabilities (Caprioli & Spitkovsky 2014*a*,*b*). The current in protons reflected at the shock dominates the reflected CR current by a factor of $\sim 5$, but in astrophysical environments, where $n_{\rm CR} \ll 0.01$, we

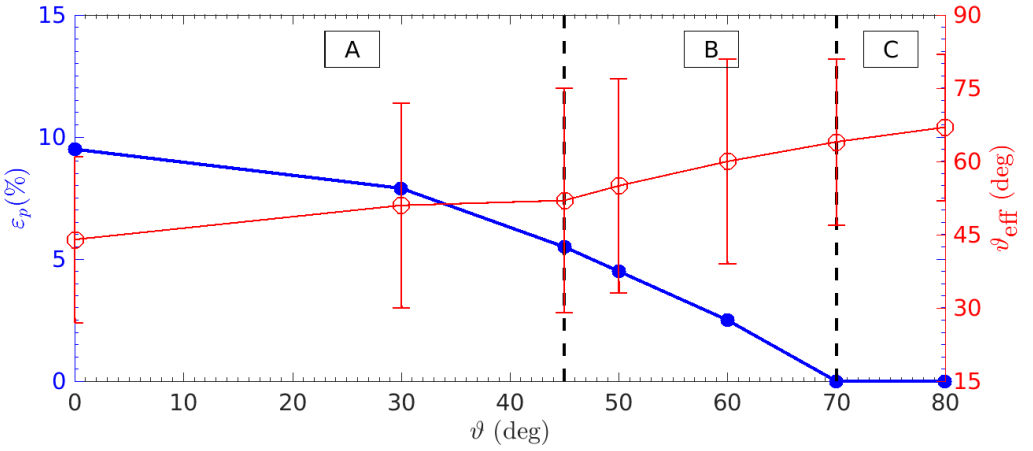


FIGURE 6. Ion acceleration efficiency $\varepsilon_{\rm p}$ as a function of the shock inclination at $M = 30$ (left axis, blue), along with the average upstream field inclination after the onset of the Bell instability (right axis, red). The filling fraction of quasi-parallel regions decreases with increasing $\vartheta$ and vanishes for $\vartheta \gtrsim 70°$. We distinguish three regimes. A: $\vartheta \leqslant 45°$, where proton DSA if efficient regardless of the presence of CRs; B: $45° \lesssim \vartheta \lesssim 60°$, where CR DSRA boosts the proton DSA efficiency; C: $\vartheta \geqslant 70°$, where even in the presence of CRs, ion DSA is absent.

expect the proton current to vastly dominate the CR current. This explains the agreement of the ion acceleration efficiency with previous simulations without CRs.

• Regime B, $50° \lesssim \vartheta \lesssim 60°$: the proton acceleration efficiency may be larger when seeds are present, because their reacceleration provides a minimum level of current in the upstream. In reality, also the fraction of reflected protons is not strictly null, but drops exponentially with $\vartheta$, and such injected protons have a velocity $\sim 2v_{\rm sh}$; therefore, the rearrangement of the magnetic field inclination is expected to happen after a timescale determined by the largest of the two currents, eventually triggering a more effective proton injection into DSA.

• Regime C, $\vartheta \geqslant 70°$: the fraction of reflected protons drops below $10^{-6}$, while there is still a reflected CR current. In this regime, however, the upstream magnetic field inclination cannot be rearranged to create quasi-parallel regions when the Bell instability enters its non-linear stage. For such quasi-perpendicular shocks injection of thermal protons is always strongly suppressed, and all the non-thermal activity depends on the presence of seeds.

### 3.3. *Quasi-Perpendicular Shocks*

Since our hybrid code is non-relativistic and the speed of light $c$ is effectively infinite, we cannot study superluminal shocks, i.e., configurations in which the velocity that a particle would need to overrun the shock by moving along the upstream magnetic exceeds $c$. For non-relativistic shocks this regime is confined to almost perpendicular inclinations $\vartheta' \geqslant \arccos(v'_{\rm sh}/c)$, where primed quantities are measure in the upstream frame (see, e.g., Sironi & Spitkovsky 2009).

Let us now consider more in detail the run with $\vartheta = 80°$ in Tab. 1, which is representative of quasi-perpendicular shock configurations. Fig. 7 (Fig. 9) shows the phase space and the time evolution of the downstream proton (CR) spectrum for such a quasi-perpendicular shock. The proton spectrum shows the characteristic supra-thermal bump found in simulations without seeds CRs (Caprioli & Spitkovsky 2014*a*), but only

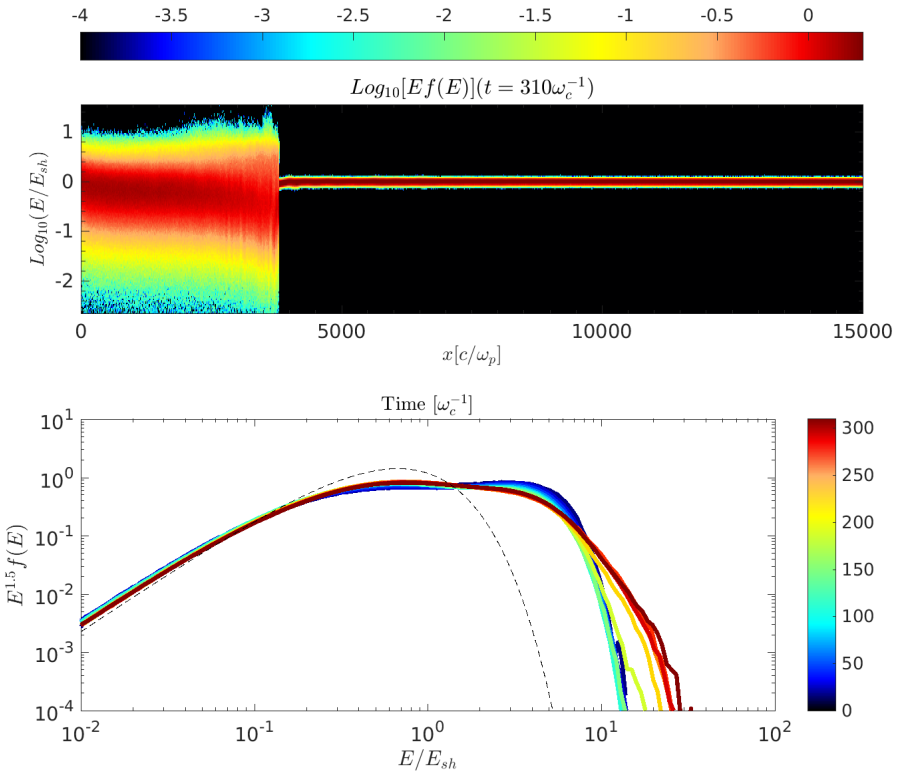


FIGURE 7. Top panel: late-time proton energy phase space for $\vartheta = 80°$. Bottom panel: time evolution of the downstream proton spectrum; the dashed line corresponds to the thermal distribution. Note that the maximum energy and the fraction of non-thermal ions grows with time after the onset of the Bell instability at $\tau_{\rm Bell} \approx 100\omega_c^{-1}$, but there are any energetic proton in the upstream, so DSA is ruled out as the acceleration process.

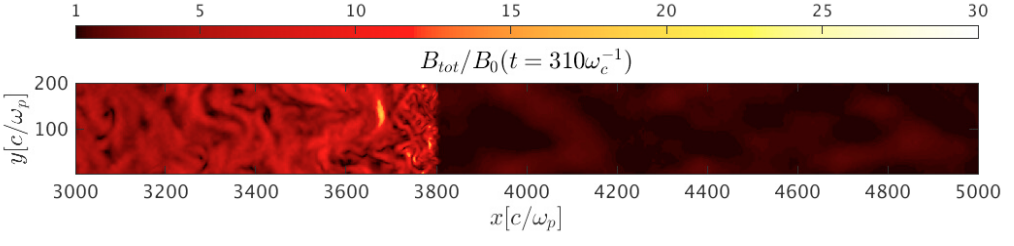


FIGURE 8. Magnetic field amplitude map around the quasi-perpendicular shock at $t = 310\omega_c^{-1}$, the time corresponding to phase space plots in Fig. 7 and Fig. 9. Note the non-linear upstream field amplification characteristic of the Bell instability driven by reaccelerated CRs and the turbulent downstream medium.

at early times. At later times, after the CR-driven Bell instability develops, both the maximum energy of the ion spectrum and the fraction of non thermal protons with $E \gtrsim 10E_{\rm sh}$ grow. However, the top panel of Fig. 7 shows no energetic protons diffusing in front of the shock, so DSA cannot be responsible for such an energization. The presence of CR-driven magnetic turbulence (shown in Fig. 8) may provide an extra source of energy available to post-shock protons, likely via magnetic reconnection. This is the first time

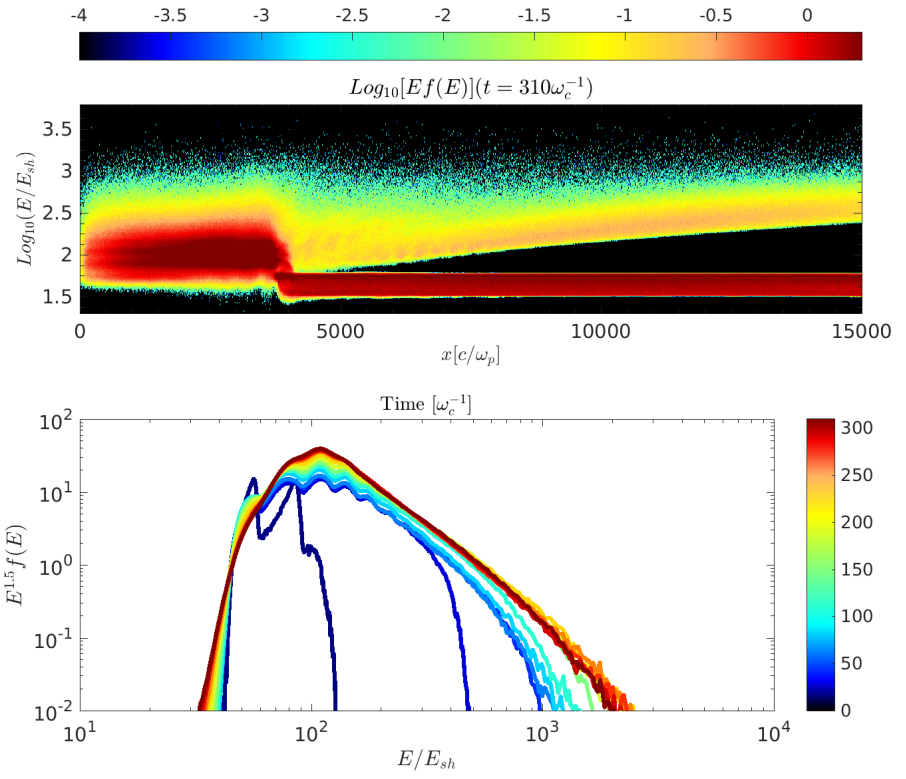


FIGURE 9. As in Fig. 7, but for CR seeds instead of protons. In this case there is a population of high-energy CRs escaping from the shock (top panel). Seeds are reaccelerated and form a power-law distribution that flattens with time and converges to $f(E) \propto E^{-4}$, significantly steeper than the DSA prediction, likely because of the larger fraction of particles that are removed by the acceleration process by being swept downstream (Bell *et al.* 2011).

that such kind of acceleration for quasi-perpendicular shocks is reported in the literature; a more detailed analysis including particle tracking is needed to fully characterize it.

Fig. 9 shows that, unlike protons, energetic ($E \gtrsim 300E_{\rm sh}$) CRs can escape upstream (top panel) and be accelerated by being scattered back and forth around the shock. The CR spectrum quickly develops a non-thermal tail, whose extent increases with time and whose slope converges to $f(E) \propto E^{-4}$, significantly steeper than the standard DSA prediction. Since power-law distributions arise from the balance between acceleration rate and escape (Bell 1978), a possible explanation for such a steep spectrum is that the quasi-perpendicular shock geometry tends to trap and advect away from the shock a fraction of diffusing particles larger than at lower-inclination shocks. This effect, which involves higher-order terms in the anisotropy expansion of the CR distribution, has been studied, e.g., by Bell *et al.* (2011), but a direct comparison with such a formalism goes beyond the goal of this paper.

We can summarize the analysis of quasi-perpendicular shocks by remarking that, in the presence of CR seeds that can be reaccelerated and drive the Bell instability, two new acceleration features appear. First, thermal protons can be accelerated in the downstream beyond the limit imposed by SDA, likely via either magnetic reconnection or second-order Fermi acceleration in the self-generated magnetic turbulence. Second, CR DSRA leads

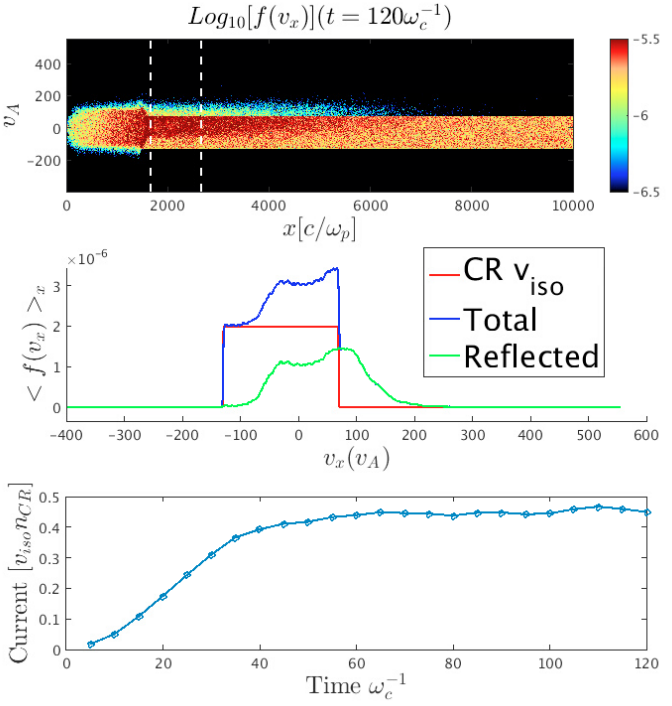


FIGURE 10. Current in reflected CRs for a shock with $\vartheta = 60°$, $M = 30$, and for $v_{\rm CR} = 100 v_A$. Top panel: $x - p_x$ CR phase space; the current is calculated immediately upstream of the shock, between vertical dashed lines. Middle panel: Distribution of reflected CRs (green line), obtained as the difference between the total one (blue) and the initial isotropic one (red). Bottom panel: time evolution of the reflected CR current, which saturates to $J_{\rm CR} \sim 0.5 e n_{\rm CR} v_{\rm CR}$ after $\sim 50\omega_c^{-1}$.

to spectra significantly steeper than the standard prediction that hinges on isotropic particle distributions.

## 4. A Universal Current in Reflected CRs

We have already outlined the crucial role played by the Bell instability generated by the reflected CR current $J_{\rm CR}$, which we want to characterize in terms of the initial CR density and velocity, and of the shock parameters such as $M$ and $\vartheta$. In other words, we now calculate the reflectivity of the shock for impinging CRs, both in terms of fraction of reflected CRs and of reflected current $J_{\rm CR} = \chi e n_{\rm CR} v_{\rm sh}$.

For such analysis we use periodic left and right boundary conditions for the CRs to ensure that an isotropic CR distribution velocity distribution impinges on the shock even at early times, when the shock is still forming. With open boundary conditions, in fact, CRs can gyrate out the left boundary and leave without replenishing the supply of positive velocity particles ahead of the shock, breaking the CR velocity isotropy in front of the shock. Periodic left and right boundary conditions for the CRs circumvent this problem as the flow of positive-velocity CRs from the right boundary ensures that the pre-shock CR distribution is indeed isotropic since the very beginning. Once the shock moves away from the wall more than a few CR gyroradii, both open and periodic boundary conditions become equivalent. After this transient, $J_{\rm CR}$ achieves a value that remains constant until $\tau_{\rm Bell}$, when non-linear perturbations start scattering CRs in pitch

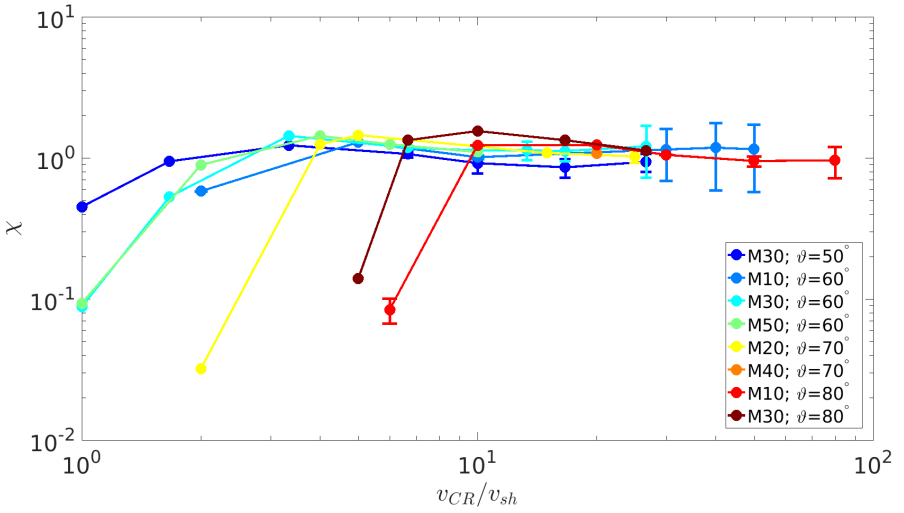


FIGURE 11. Current in reflected CRs as a function of $v_{\rm CR}/v_{\rm sh}$ for shocks with different Mach numbers and field inclinations, as in the legend. For $v_{\rm CR} \gg v_{\rm sh}$, the reflected current $J_{\rm CR} \simeq e n_{\rm CR} v_{\rm sh}$, independent of $M$ and $\vartheta$. For $v_{\rm CR}$ less than a few times $v_{\rm sh}$, $J_{\rm CR}$ drops steeply, and the location of such a drop depends strongly on the field inclination, consistent with the expectations for supra-thermal particles (Caprioli *et al.* 2015).

angle. We choose a low CR number density of $n_{\rm CR} = 4 \times 10^{-4}$ to have time to measure the saturation of the shock reflectivity before the onset of non-linear phenomena.

The current $J_{\rm CR}$ is directed along the positive $x-$axis and can be calculated by looking at the $x-p_x$ phase space and integrating in $v_x$ the difference between the total distribution function $f(v_x)$ and the initial isotropic function, which is flat between $-v_{\rm CR}$ and $+v_{\rm CR}$ (we use also $v_{\rm iso} \equiv v_{\rm sh}$). Fig. 10 shows the results of such a calculation for a case with $M = 30$, $\vartheta = 60°$, and $v_{\rm CR} = 100 v_A$. From the middle panel we see that the distribution of reflected CRs $f^r_{CR}$ (green line) peaks slightly below $+v_{\rm CR}$, with asymmetrical tails between $-v_{\rm CR}$ and $+2v_{\rm CR}$. The bottom panel of Fig. 10 shows that the CR current saturates for $t \gtrsim 50\omega_c^{-1}$, much earlier than the onset of the Bell instability. From the plots in Fig. 10, we also determine the fraction of reflected CRs $\eta$, defined as

$$\eta \equiv \frac{\int f^r_{CR}(v_x) dv_x}{\int f^{iso}_{CR}(v_x) dv_x} \tag{4.1}$$

and the average velocity of the reflected CRs

$$v_r \equiv \langle v_x \rangle \equiv \frac{J_{\rm CR}}{\eta e n_{\rm CR}}. \tag{4.2}$$

Fig. 11 shows the normalized CR current $\chi$ as a function of $v_{\rm CR}$ for a range of Mach numbers and oblique to quasi-perpendicular field inclinations. Remarkably, for large values of $v_{\rm CR}/v_{\rm sh}$, $\chi$ approaches unity regardless of the shock properties. The very reason for such a universality can be understood by separating the contributions of $\eta$ and $v_r$, as illustrated in Fig. 12. The shock reflectivity (left panel) naturally drops if $v_{\rm CR} \lesssim$ a few times $v_{\rm sh}$, where the post-reflection velocity is smaller than the injection velocity, which strongly depends on the shock inclination (Caprioli *et al.* 2015). At the same time, $\eta$ decreases almost linearly for $v_{\rm CR} \gg v_{\rm sh}$ because very energetic particles with large rigidities tend not to see the shock discontinuity. The peak of reflectivity depends on the

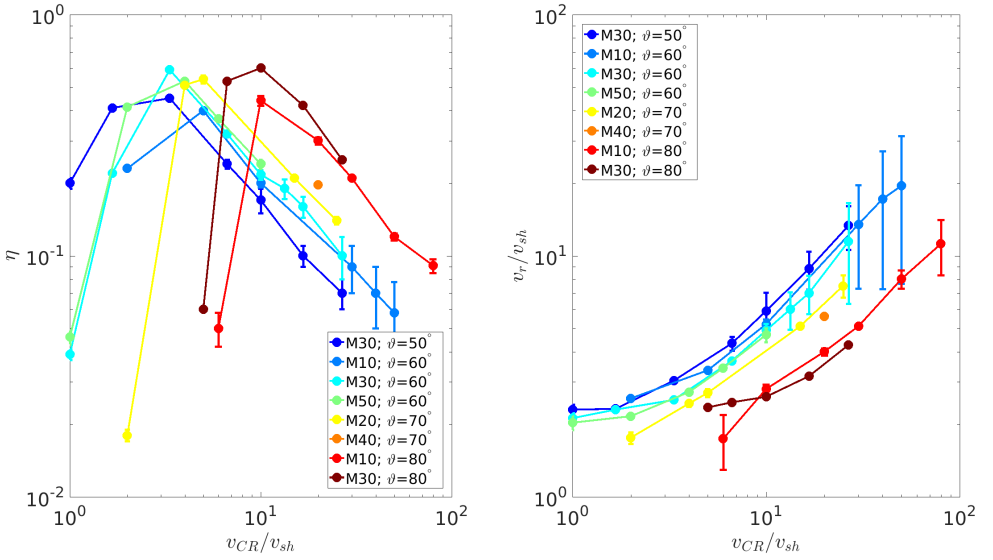


FIGURE 12. Left panel: Fraction $\eta$ of CRs reflected at the shock. $\eta$ increases for larger $\vartheta$, and decreases steeply for $v_{\rm CR}$ less than a few times $v_{\rm sh}$ and linearly for $v_{\rm CR} \gg v_{\rm sh}$. Right panel: average velocity of reflected CRs $v_r$, which decreases with $\vartheta$ and increases linearly for $v_{\rm CR} \gtrsim v_{\rm sh}$. The combination of such trends returns the constant $J_{\rm CR}$ in Fig. 11.

shock inclination, and increases with $\vartheta$ at fixed $v_{\rm CR}/v_{\rm sh}$, because the more oblique shock effectively "shrinks" the CR gyroradius. The suppression of $\eta$ for $v_{\rm CR} \gg v_{\rm sh}$ is exactly compensated by the linear increase of $v_r$, which is just proportional to $v_{\rm CR}$ (right panel of Fig. 11). Finally, at fixed $v_{\rm CR}$, $v_r$ decreases for large inclinations because CRs stream along the field lines, and a higher field inclination means a lower $x$ velocity.

In summary, for $v_{\rm CR} \gg v_{\rm sh}$ we expect a universal current due to reflected CRs, which has a very simple and elegant expression

$$J_{\rm CR} \simeq e n_{\rm CR} v_{\rm CR} \qquad \chi \simeq 1. \tag{4.3}$$

Such a current arises from the exact balance of the dependence of both $\eta$ and $v_r$ on $\vartheta$ and $v_{\rm CR}/v_{\rm sh}$, and has a profound meaning, as we outline in the next section.

### 4.1. *Derivation of the Universal CR Current*

Let us define coordinates in the shock frame such that the shock is at $x = 0$, $x < 0$ is upstream, and $x > 0$ is downstream. Let primed quantities denote the upstream frame and unprimed quantities denote the shock frame. In the upstream frame, the shock moves at $-v_{\rm sh}\hat{x}$ and the isotropic CR distribution function reads $f'(\mu') = \frac{n_{\rm CR}}{2}$, where $\mu$ is the cosine of the angle between the CR velocity vector and the $x$ axis. Conservation of particle number requires that

$$f'(\mu')d\mu' = f(\mu)d\mu, \tag{4.4}$$

and in the limit of CR velocity $v \gg v_{\rm sh}$ one has $d\mu \approx d\mu'$, and eventually $f'(\mu') \approx f(\mu)$.

In the shock frame the particle flux is conserved, i.e.,

$$J_u + J_{in} + J_r = J_d, \tag{4.5}$$

where $J_u(J_d)$ is the current at upstream (downstream) infinity, $J_{in}$ is the current

impinging on the shock, and $J_r$ is the reflected current, which we want to calculate. In the shock frame, the upstream CR velocity along $x$ is $v_u = v\mu + v_{\rm sh}$ and we have

$$J_u + J_{in} = e\int_{v_u<0} d\mu f(\mu)(\mu v + v_{\rm sh}) + e\int_{v_u>0} d\mu f(\mu)(\mu v + v_{\rm sh}) \tag{4.6}$$

$$\approx \frac{en_{\rm CR}}{2}\left(\int_{-1}^{-v_{\rm sh}/v} d\mu(\mu v + v_{\rm sh}) + \int_{-v_{\rm sh}/v}^{1} d\mu(\mu v + v_{\rm sh}))\right) = en_{\rm CR}v_{\rm sh} \tag{4.7}$$

and eventually

$$J_r = J_d - en_{\rm CR}v_{\rm sh}. \tag{4.8}$$

Since in the upstream frame $J' = J - en_{\rm CR}v_{\rm sh}$, there the reflected current reads

$$J'_r = J_d - 2en_{\rm CR}v_{\rm sh}. \tag{4.9}$$

This is exactly the quantity that we measured above as $J_{\rm CR} \simeq en_{\rm CR}v_{\rm sh}$, modulo a sign flip that comes from the new orientation of the $x-$axis. By posing $J'_{ref} = -J_{\rm CR}$ we finally derive $J_d = en_{\rm CR}v_{\rm sh}$, which implies $J_r = 0$.

In the shock frame, having $J_r = 0$ and $J_u + J_{in} = J_d = en_{\rm CR}v_{\rm sh}$ simply means that the shock is "transparent" to CRs with $v \gg v_{\rm sh}$. Here "transparent" means that the anisotropy of the CR distribution is preserved across the shock, not that no CRs reflect at the shock front. One could have come to the same conclusion by assuming that, in the limit of $v_{\rm CR} \gg v_{\rm sh}$, CRs have Larmor radii much larger than the shock thickness, so the shock has a negligible affect on their overall distribution, the same reasoning used when solving the CR transport equation analytically. Requiring that the CR distribution in the shock frame remains the same after passage from upstream to downstream requires $J_r = 0$, and this induces a net current $n_{\rm CR}v_{\rm CR}$ in the upstream frame, a current that can be used to drive plasma instabilities in the upstream plasma. From the microphysical point of view, it is useful stress that such a current is comprised of less than $n_{\rm CR}$ CRs that can overrun the shock because their velocities are larger than $v_{\rm sh}$.

## 5. Application to SNRs

We now make use of the fact that the reflected CR current is $J_{\rm CR} = en_{\rm CR}v_{\rm sh}$ to calculate the expected growth time of the Bell instability at SNR shocks due to the reacceleration of Galactic CRs.

We start from the flux of Galactic CRs measured by the Voyager I spacecraft (Stone *et al.* 2013) and consider the non-relativistic part of such a flux, since it encompasses most of the particle number density. The transformation from energy flux to momentum distribution can be performed by exploiting

$$4\pi p^2 f(p)dp = \frac{4\pi}{v(p)}\phi(E)dE. \tag{5.1}$$

For non relativistic particles $E \sim p^2$ so $dp/dE \sim p^{-1}$. As $v(p) \sim p$, $f(p) \sim p^{-2}$. Thus, the complete expression for the seed momentum distribution at low energies is

$$f_{CR}(p) = \frac{10^{-9}}{cm^3}\frac{1}{4\pi}p_0^{-3}\left(\frac{p}{p_0}\right)^{-2}. \tag{5.2}$$

where $p_0 = \gamma mc \sim mc$ and we scaled the normalization to the typical CR energy density of $1{\rm eV/cm}^3$. Such non-relativistic CR spectrum is rather hard, scaling as $p^{-2}$, and sets the level of seeds that can be reprocessed by SNR shocks. This scaling extends down to

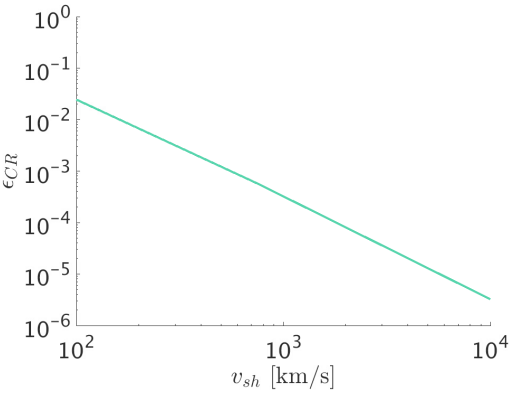


FIGURE 13. Expected CR acceleration efficiency $\varepsilon_{\rm CR}$ as a function of the SNR shock velocity, assuming the typical diffuse spectrum of GCRs. In slow shocks with $v_{\rm sh} \gtrsim 100$km/s $\varepsilon_{\rm CR}$ can be as large as a few per cent, while for $v_{\rm sh} \gtrsim 1000$km/s $\varepsilon_{\rm CR}$ drops considerably.

MeV protons, which have $v \sim v_{\rm sh}$, and can be integrated to find $n_{\rm CR}$ as

$$n_{\rm CR} = \int_{p_{min}}^{mc} 4\pi p^2 \left[ \frac{10^{-9}}{cm^3} \frac{1}{4\pi} p_0^{-3} \left( \frac{p}{p_0} \right)^{-2} \right] dp = \frac{10^{-9}}{cm^3} \left( 1 - \frac{3v_{\rm sh}}{c} \right). \tag{5.3}$$

We have assumed $p_{min} \simeq 3mv_{\rm sh}$ for the injection momentum based on our previous hybrid simulations (Caprioli & Spitkovsky 2014*a*; Caprioli *et al.* 2015), but also on the fact that $p_{min}$ is where the constant scaling of $J_{\rm CR}$ with $v_{\rm CR}/v_{\rm sh}$ starts.

For $v_{\rm sh} \sim 10^4$km/s, one obtains $n_{\rm CR} \sim 9 \times 10^{-10} cm^{-3}$, much smaller the values used in the paper. Finally, by using Eq. 2.3, for $B_0 = 3\mu$G and $n_p = 1 cm^{-3}$ we get $\omega_c^{-1} \sim 35$s and $\tau_{\rm Bell} \sim 3 \times 10^8$s $\sim 10$yr. This timescale is much shorter that the typical dynamical SNR time of thousands of years, suggesting that the Bell instability has ample time to grow and amplify the upstream **B** field to nonlinear levels.

Given the universality of the CR reacceleration efficiency of $\sim 10\%$ for our reference parameters ($n_{\rm CR} = 0.01$ and $v_{\rm CR} = 50 v_A$, see Fig. 5), we can estimate the CR DSRA efficiency for a range of shock velocities simply by rescaling $n_{\rm CR}$ to the actual value for Galactic CRs. Fig. 13 shows gives $\varepsilon_{\rm CR}$ for typical interstellar values of $n_p = 1$ cm$^{-3}$, $n_{\rm CR} = 10^{-9}$cm$^{-3}$, $v_A \sim 10$km/s, $v_{\rm CR} = c$, and $v_{\rm sh} = 100 - 10,000$ km/s. The CR reacceleration efficiency ranges from $\varepsilon_{\rm CR} \simeq 2\%$ for $v_{\rm sh} = 100$km/s to $\varepsilon_{\rm CR} \simeq 3 \times 10^{-6}$ for $v_{\rm sh} = 10,000$km/s, suggesting that DSRA may be important for middle-age and old SNR in the late-Sedov or radiative stages.

Another case in which CR reacceleration is expected to be important is when SNR shocks encounter dense molecular clouds, as in W44 or IC443, which are prominent sources of hadronic $\gamma-$rays (Ackermann et al. 2013). As shown by different authors (Uchiyama *et al.* 2010; Cardillo *et al.* 2016), the observed $\gamma-$ray spectrum can be explained without invoking DSA of thermal protons but as simply due to the re-acceleration of the low-energy Galactic CRs that should be trapped inside the molecular clouds. By assuming that the density of CRs is proportional to the gas density, in dense clouds one would infer $n_{\rm CR}$ few orders of magnitude larger than the estimate in Eq. 5.3. Moreover, since these SNRs are quite old, their $v_{\rm sh} \approx 200 - -500$km/s fall exactly in the regime where DSRA is expected to be more efficient in units of $nv_{\rm sh}^2$ (Fig. 13). The combination of these two factors suggests that in dense clouds the DSRA efficiency can easily be larger that 10–20%, beyond which the modification induced by non-thermal particles smoothens the shock transition, in turn suppressing injection and seed reflection.

## 6. Conclusions

We have presented the first comprehensive set of hybrid simulations that address the reacceleration of pre-existing energetic particles in non-relativistic collisionless shocks and its effects on the global shock dynamics, in particular on proton injection and acceleration. Our findings are summarized here in the following.

- Seeds with sufficiently-large energy (a few times $v_{\rm sh}$, depending on the shock inclination) are effectively reflected at the shock, creating a current that can drive unstable Bell modes in the upstream medium; Seeds can then be scattered back and forth across the shock, diffusing on the self-generated magnetic turbulence, and develop power-law tails via a process that we call DSRA (Fig. 1).
- Once the Bell instability enters its non-linear stage, the effective shock inclination changes (Fig. 2). At oblique shocks ($50 \lesssim \vartheta \lesssim 70^\circ$), where proton injection is normally inhibited (Caprioli & Spitkovsky 2014*a*; Caprioli *et al.* 2015), the field rearrangement opens up quasi-parallel patches in front of the shock where also thermal protons can be injected into DSA (Fig. 2).
- For quasi-perpendicular shocks ($\vartheta \gtrsim 70^\circ$), seeds can still drive Bell waves and undergo DSRA, but injection of thermal protons is always suppressed (Fig. 6). However, in this regime two new phenomena happen: first, protons are accelerated in the downstream thanks to the CR-driven turbulence (Fig. 7); second, seeds are accelerated via DSRA with a $E^{-4}$ spectrum much steeper than the universal DSA prediction (Fig. 9).
- For $v_{\rm CR} \gg v_{\rm sh}$, the current in reflected CRs has a universal character, and reads $J_{\rm CR} \simeq e n_{\rm CR} v_{\rm CR}$, independently of shock Mach number, inclination, and $n_{\rm CR}$ (Fig. 11). Simulations and theory (§4) explain this in terms of conservation of the seed anisotropy in the shock crossing, in the shock frame, in the limit in which the seed gyroradii are much larger than the shock thickness.
- For SNR shocks propagating into the interstellar medium filled with Galactic CRs, the growth time of the Bell instability due solely to the universal current in reflected CRs is of order of a few years only; this means that a minimum level of magnetic field amplification at SNR shocks must be expected, regardless of the shock inclination.
- For middle-age/old SNRs with $v_{\rm sh}$ of a few hundred km/s, DSRA of Galactic CRs alone can yield a total acceleration efficiency of few per cent, which may become even larger if the shock propagates in molecular clouds where the density of low-energy CRs can be significantly larger than in the diffuse interstellar medium.

Seed reacceleration is also expected to be important in heliospheric shocks, since the solar wind typically contains energetic particles that are pre-accelerated, for instance, in solar flares. In these cases, the peculiar chemical composition observed in solar energetic particle events (e.g., Mason *et al.* 2004; Tylka *et al.* 2005) represents a powerful diagnostics for investigating the interplay between shock inclination, seed reacceleration, and thermal particle acceleration. We also stress the analogies between the efficient reacceleration of energetic seeds and the preferential acceleration of ions with large mass/charge ratios (Caprioli *et al.* 2017), since both particles share the property of having gyroradii (much) larger than thermal protons.

Finally, it is worth mentioning that, while in our hybrid simulations we can only account for seed ions, the same reacceleration mechanisms described in the paper should apply also to seed electrons with large gyroradii. This may have phenomenological implications for the multi-wavelength emission of middle-age SNRs and be important for interpreting spacecraft observations of energetic electrons.

This research was supported by NASA (grant NNX17AG30G to DC), NSF (grant AST-1517638 to AS), and Simons Foundation (grant 267233 to AS). Simulations were

performed on computational resources provided by the Princeton High-Performance Computing Center, the University of Chicago Research Computing Center, and XSEDE TACC (TG-AST100035).

## REFERENCES

Ackermann et al., M. 2013 Detection of the Characteristic Pion-Decay Signature in Supernova Remnants. *Science* **339**, 807–811, arXiv: 1302.3307.

Amato, E. & Blasi, P. 2009 A kinetic approach to cosmic-ray-induced streaming instability at supernova shocks. *MNRAS* **392**, 1591–1600, arXiv: 0806.1223.

Bell, A. R. 1978 The acceleration of cosmic rays in shock fronts. I. *MNRAS* **182**, 147–156.

Bell, A. R. 2004 Turbulent amplification of magnetic field and diffusive shock acceleration of cosmic rays. *MNRAS* **353**, 550–558.

Bell, A. R., Schure, K. M. & Reville, B. 2011 Cosmic ray acceleration at oblique shocks. *MNRAS* **418**, 1208–1216, arXiv: 1108.0582.

Blasi, P. 2004 Nonlinear shock acceleration in the presence of seed particles. *APh* **21**, 45–57, arXiv: astro-ph/0310507.

Caprioli, D. 2015 Cosmic-ray acceleration and propagation. In *34th International Cosmic Ray Conference (ICRC2015)*, *International Cosmic Ray Conference*, vol. 34, p. 8, arXiv: 1510.07042.

Caprioli, D., Amato, E. & Blasi, P. 2010 The contribution of supernova remnants to the galactic cosmic ray spectrum. *APh* **33**, 160–168, arXiv: 0912.2964.

Caprioli, D., Pop, A. & Spitkovsky, A. 2015 Simulations and Theory of Ion Injection at Non-relativistic Collisionless Shocks. *ApJL* **798**, 28, arXiv: 1409.8291.

Caprioli, D. & Spitkovsky, A. 2013 Cosmic-Ray-induced Filamentation Instability in Collisionless Shocks. *ApJL* **765**, L20, arXiv: 1211.6765.

Caprioli, D. & Spitkovsky, A. 2014*a* Simulations of Ion Acceleration at Non-relativistic Shocks: I. Acceleration Efficiency. *ApJ* **783**, 91, arXiv: 1310.2943.

Caprioli, D. & Spitkovsky, A. 2014*b* Simulations of Ion Acceleration at Non-relativistic Shocks: II. Magnetic Field Amplification. *ApJ* **794**, 46, arXiv: 1401.7679.

Caprioli, D., Yi, D. T. & Spitkovsky, A. 2017 Chemical enhancements in shock-accelerated particles: Ab-initio simulations. *ArXiv e-prints* , arXiv: 1704.08252.

Cardillo, M., Amato, E. & Blasi, P. 2016 Supernova remnant w44: a case of cosmic-ray reacceleration. *A&A* **595**, A58, arXiv: 1604.02321.

Mason, G. M., Mazur, J. E., Dwyer, J. R., Jokipii, J. R., Gold, R. E. & Krimigis, S. M. 2004 Abundances of heavy and ultraheavy ions in $^3$he-rich solar flares. *ApJ* **606**, 555–564.

Morlino, G. & Caprioli, D. 2012 Strong evidence for hadron acceleration in Tycho's supernova remnant. *A&A* **538**, A81, arXiv: arXiv:1105.6342.

Reville, B. & Bell, A. R. 2013 Universal behaviour of shock precursors in the presence of efficient cosmic ray acceleration. *MNRAS* **430**, 2873–2884, arXiv: 1301.3173.

Sironi, L. & Spitkovsky, A. 2009 Particle acceleration in relativistic magnetized collisionless pair shocks: Dependence of shock acceleration on magnetic obliquity. *ApJ* **698**, 1523–1549, arXiv: 0901.2578.

Skilling, J. 1975 Cosmic ray streaming. I - Effect of Alfven waves on particles. *MNRAS* **172**, 557–566.

Stone, E. C., Cummings, A. C., McDonald, F. B., Heikkila, B. C., Lal, N. & Webber, W. R. 2013 Voyager 1 observes low-energy galactic cosmic rays in a region depleted of heliospheric ions. *Science* **341**, 150–153.

Tylka, A. J., Cohen, C. M. S., Dietrich, W. F., Lee, M. A., Maclennan, C. G., Mewaldt, R. A., Ng, C. K. & Reames, D. V. 2005 Shock Geometry, Seed Populations, and the Origin of Variable Elemental Composition at High Energies in Large Gradual Solar Particle Events. *ApJ* **625**, 474–495.

Uchiyama, Y., Blandford, R. D., Funk, S., Tajima, H. & Tanaka, T. 2010 Gamma-ray emission from crushed clouds in supernova remnants. *ApJL* **723**, L122–L126, arXiv: 1008.1840.